Spin-Crossover Behavior in the $Fe(tap)_2(NCS)_2 \cdot n CH_3CN$ System (tap = 1,4,5,8-Tetraazaphenanthrene; $n = 1, {}^1/_2$). Crystal Structures and Magnetic Properties of Both Solvates

José Antonio Real,*[1a] M. Carmen Muñoz,[1b] Enrique Andrés,[1a] Thierry Granier,*[1c] and Bernard Gallois[1c]

Departament de Química Inorgànica, Universitat de València, Dr. Moliner 50, 46100 Burjassot (València), Spain, Departamento de Física Aplicada, Universidad Politécnica de Valencia, Camino de Vera s/n, 46071 Valencia, Spain, and Laboratoire de Cristallographie et de Physique Cristalline, Université Bordeaux I, 351 Cours de la Liberation, 33405 Talence, France

Received February 9, 1994[⊕]

The synthesis, structure, and magnetic characterization of two solvates of bis(1,4,5,8-tetraazaphenanthrene)bis(thiocyanato)iron(II), $[Fe(tap)_2(NCS)_2] \cdot n CH_3CN$ with $n = 1$ (solvate A) and $n = {}^1/_2$ (solvate B) are reported. A shows a continuous high-spin ↔ low-spin conversion over the temperature range ca. 110–280 K, while B is paramagnetic over the temperature range 4.2–290 K. The X-ray structure for A was solved at 290 and 135 K. It crystallizes in the triclinic space group $P\bar{1}$ with $Z = 2$ at both temperatures. The lattice constants are $a = 8.920(3)$ Å, $b = 9.372(3)$ Å, $c = 16.838(4)$ Å, $\alpha = 96.32(2)°$, $\beta = 100.47(3)°$, $\gamma = 112.14(2)°$, and $V = 1257.3$ Å^3 at 290 K and $a = 8.742(2)$ Å, $b = 9.265(2)$ Å, $c = 16.535(3)$ Å, $\alpha = 96.56(2)°$, $\beta = 100.15(3)°$, $\gamma = 112.43(3)°$, and $V = 1194.07$ Å^3 at 135 K. The data were refined to $R = 5.67$ (290 K) and 7.57% (135 K). B crystallizes in the monoclinic space group $C2/c$, with $a = 22.636(4)$ Å, $b = 16.810(3)$ Å, $c = 18.528(3)$ Å, $\beta = 138.55\ (3)°$, and $V = 4666{,}90$ Å^3 at 290 K. The final reliability factor was $R = 5.93\%$. Molecular structures for both solvates are very similar at room temperature where iron(II) lies in a distorted octahedron with NCS^- ligands in the cis position. The most significant structural features which could account for the different magnetic behavior of A and B are found to be the metal-to-ligand bond distances and trigonal distortion. Structural modifications associated with the spin change in A mainly consist of a large reorganization of the metal environment: the Fe–N(tap) and Fe–N(CS) distances decrease by 0.23 (mean value) and 0.12 (mean value) Å, respectively, when the temperature is lowered from 290 to 135 K, and a more regular shape of the $[FeN_6]$ octahedron is achieved through a modification of the trigonal deformation from 8 to 3° along with a remarkable variation of the N–Fe–N angles. The gradual temperature dependence of $\chi_M T$ for A was considered as a Boltzmann distribution of molecules in the low-spin ground state and in the thermally accessible high-spin excited state reflecting the ${}^1A_1 \leftrightarrow {}^5T_2$ spin equilibrium. The enthalpy and entropy changes associated with the spin equilibrium were estimated as $\Delta H = 15.5$ kJ mol^{-1} and $\Delta S = 92$ J mol^{-1} K^{-1}. Analysis of the magnetic data versus temperature for B by using the zero-field-splitting spin Hamiltonian for $S = 2$ leads to $D = 7.4$ cm^{-1} and $g = 2.09$.

Introduction

The spin-crossover phenomenon requires the ligand field strength to be of the same order of magnitude as the mean electron-pairing energy. Then, high-spin (hs) and low-spin (ls) forms may interconvert, their proportion varying with temperature,[2] pressure,[3] and electromagnetic radiation.[4] In the ls state, the e_g orbitals, which have an antibonding character, are depopulated and the hs → ls crossover results in a shortening of metal–ligand bond lengths.[5]

Two closely related aspects are to be taken into account to understand the spin-crossover mechanism: (i) how the spin change occurs at a molecular level and (ii) how this change spreads in the solid to result in the different kinds of spin conversions. From a molecular point of view, due to the absence of cooperative effects, the determination of the factors that control the rate and mechanism of the spin-state interconversion in an isolated spin-crossover complex was at the origin of the spin conversion studies in solution, which are based on the observation of the relaxation of the perturbed equilibrium.[6] In the solid state, the temperature-dependent spin conversion is cooperative in nature, involving long-range interactions among the changing spin state metal complex molecules themselves as well as the latter and the lattice. Thus, spin conversion rates depend on subtle solid-state effects induced by noncoordinating counterions, noncoordinating solvent molecules, preparative methods, or ligand substitution. Hence, such factors can affect drastically the shape of the temperature variable order parameter (usually the high-spin molar fraction) and the critical temperature T_c at which the 50% of conversion takes place. So, it is possible to get spin-crossover transformations which occur abruptly in a narrow temperature range (less than 10 K) and others which occur very gradually.[7] In the latter case, each molecule in the crystal acts independently of its neighbors and there is a simple Boltzmann distribution of the high- and low-spin forms. Some papers dealing with the understanding of

⊕ Abstract published in *Advance ACS Abstracts*, June 15, 1994.

(1) (a) Universitat de València. (b) Universidad Politéctica de València. (c) Université de Bordeaux I.
(2) Gütlich, P. *Struct. Bonding (Berlin)* **1981**, *44*, 83.
(3) (a) Adams, D. M.; Long, G. J.; Williams, A. D. *Inorg. Chem.* **1982**, *21*, 1049. (b) Pebler, J. *Inorg. Chem.* **1982**, *22*, 4135. (c) Usha, S.; Srinivasan, R.; Rao, C. N. R. *Chem. Phys.* **1985**, *100*, 447.
(4) Gütlich, P.; Hauser, A. *Coord. Chem. Rev.* **1990**, *97*, 1,
(5) König, E. *Prog. Inorg. Chem.* **1987**, *35*, 527.
(6) (a) Beattie, J. K. *Adv. Inorg. Chem.* **1988**, *32*, 2. (b) Toftlund, H. *Coord. Chem. Rev.* **1989**, *94*, 67. (c) Konig, E. *Struct. Bonding (Berlin)* **1991**, *76*, 51.
(7) König, E.; Ritter, G.; Kulshrestha, S. K. *Chem. Rev.* **1985**, *85*, 219.

0020-1669/94/1333-3587$04.50/0

the molecular mechanism involved in fast hs ↔ ls interconversion leading to spin equilibrium were reported recently.[8]

The most abrupt spin conversions reported up to now are those exhibited by a number of iron(II) complexes.[2] Among these systems, $[Fe(phen)_2(NCS)_2]$ (phen 1,10-phenanthroline), which undergoes an abrupt hs ↔ ls transition at a temperature $T_c = 176$ K, has certainly been one of the most investigated iron(II) spin transition complexes. Only very recently, it has been possible to carry out on this system a single-crystal X-ray structural study[9] and a thermal expansion investigation[10] as well as the first X-ray single-crystal structure determination as a function of pressure[11] at room temperature for a spin-crossover system. All these studies aimed at finding the factors which determine the spin interconversion mechanism.

The present work was undertaken mainly to study the influence of a modification of the phen ligand on the spin transition of $[Fe(phen)_2(NCS)_2]$. In this respect, it deserves to be noted that although the effects of replacing hydrogen atoms by electron-donating, electron-withdrawing, or simply bulky ligands in phen were widely studied a long time ago,[2] the substitution of two C–H groups of phen by two additional more electronegative nitrogen atoms was unknown. Along this line, we report here the synthesis, magnetic characterization, and structural investigation of the system $[Fe(tap)_2(NCS)_2]\cdot nCH_3CN$, where tap is the 1,4,5,8-tetraazaphenanthrene (see scheme I) and $n = 1$ (A) and 0.5 (B).

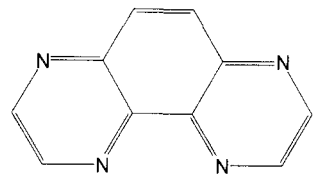

I

A is a spin-crossover system whereas B is a high-spin one. As the crystal structures of both solvates have been solved, this work is a good opportunity to analyze and discuss the relationships between structural factors on the occurrence of spin-crossover.

Experimental Section

Materials. $[Fe(py)_4(NCS)_2]$ (py = pyridine) was prepared according to the method described by Erickson and Sutin,[12] the hydrated iron(II) perchlorate salt being replaced by the hydrated iron(II) sulfate one. Tap ligand was purchased from commercial sources and used without further purification.

Complex Preparation. $[Fe(tap)_2(NCS)_2]\cdot nCH_3CN$ was synthesized under argon atmosphere as follows: previously deoxygenated acetonitrile solutions of $[Fe(py)_4(NCS)_2]$ (0.27 mmol, 40 mL) and tap (0.55 mmol, 10 mL) were mixed under stirring at room temperature. Polyhedral ($n = 1$, A) and prismatic ($n = 0.5$, B) dark single crystals were obtained by slow evaporation of the purple solution 2 weeks later. They were dried under argon atmosphere and were used for X-ray diffraction and magnetic studies.

Magnetic Susceptibility Measurements. They were performed on crystalline samples weighing 5.48 and 4.59 mg for A and B, respectively, over the temperature range 295–4.5 K, by using a Faraday-type cryostat. The independence of susceptibility on the applied magnetic field was checked for each compound at room temperature. Mercury tetrakis(thiocyanato)cobaltate(II) was used as a susceptibility standard. Diamagnetic corrections[13] were estimated to be -332×10^{-6} and -321×10^{-6} cm^3 mol^{-1} for A and B, respectively. The temperature was varied at a rate of 1 K min^{-1}.

Table 1. Crystallographic Data for $Fe(tap)_2(NCS)_2\cdot CH_3CN$ ($C_{24}H_{15}N_{11}S_2Fe$; $M_r = 576.85$)

	290 K	135 K
a, Å	8.920(3)	8.742(2)
b, Å	9.372(3)	9.265(2)
c, Å	16.838(4)	16.535(3)
α, deg	96.32(2)	96.56(2)
β, deg	100.47(2)	100.15(3)
γ, deg	112.14(2)	112.14(2)
V, Å^3	1257.30	1194.07
Z	2	2
space group	$P\bar{1}$	$P\bar{1}$
$\lambda_{CuK\alpha}$, Å	1.5418	
ρ_{obs}, g cm^3	1.525	1.605
μ, cm^{-1}	32.60	32.60
R^a	0.0567	0.0757
$R_w{}^a$	0.0583	0.0790

$^a R = \sum[|F_o| - |F_c|]/\sum|F_o|$. $R_w = \sum w^{1/2}[|F_o| - |F_c|]/\sum w^{1/2}|F_o|$.

Table 2. Crystallographic Data for $Fe(tap)_2(NCS)_2\cdot{}^1/_2CH_3CN$

chemical formula $C_{23}H_{23.5}N_{10.5}S_2Fe$	space group $C2/c$
$a = 22.636(4)$ Å	$T = 290$ K
$b = 16.810(3)$ Å	$\lambda_{CuK\alpha} = 1.5418$ Å
$c = 18.528(3)$ Å	$\rho_{obs} = 1.585$ g cm^{-3}
$\beta = 138.55(3)°$	$\mu = 34.87$ cm^{-1}
$V = 4666.90$ Å^3	$R^a = 0.0593$
$Z = 8$	$R_w{}^a = 0.0626$
$M_r = 556.35$	

$^a R = \sum[|F_o| - |F_c|]/\sum|F_o|$. $R_w = \sum w^{1/2}[|F_o| - |F_c|]/\sum w^{1/2}|F_o|$.

Solution and Refinement of the X-ray Structures. Preliminary X-ray investigations have been performed by usual photographic methods. Concerning crystal solvate A, low-temperature X-ray diffraction experiments were conducted by cooling the sample with a cold nitrogen gas flow surrounded by a jacket of dry nitrogen gas at room temperature, which prevents frost from growing around the sample. Data collections were carried out on an Enraf-Nonius CAD4 diffractometer with monochromatized Cu Kα radiation. Crystal sizes were $0.10 \times 0.10 \times 0.30$ and $0.20 \times 0.12 \times 0.30$ mm for A and B, respectively. Details concerning crystal data, data collection characteristics, and structure refinement are summarized in Tables 1 and 2. Lattice parameters were obtained from least squares refinement of the setting angles of 25 reflections in the range $15 < \theta < 25°$. Lorentz–polarization and absorption corrections were applied. Room-temperature structures for A and B were solved by direct methods using SHELX86[14] and refined by full-least squares refinement using SHELX76.[15] Atomic scattering factors were taken from ref 16. The low-temperature structure of A was refined by starting with the values of the atomic coordinates at room temperature. Final refinement by minimizing the function $\sum w(F_o - F_c)^2$ converged to $R = 0.0567$ ($R_w = 0.0583$) and $R = 0.0757$ ($R_W = 0.0790$) for the room- and low-temperature structures of A. Concerning the room-temperature structure of B, final reliability factors were $R = 0.0593$ and $R_w = 0.0626$. Non-hydrogen atoms were refined anisotropically for both compounds. All hydrogen atoms were placed in computed positions and isotropically refined. Fractional atomic coordinates and selected bond distances and angles for A and B are given in Tables 3–6.

Results and Discussion

Description of the Structures. Structure of A at 290 K. Crystal solvate A crystallizes in the triclinic $P\bar{1}$ space group. The unit cell contains two $[Fe(tap)_2(NCS)_2]$ and two CH_3CN molecules.

(8) (a) Chang, H.; McCusker, J. K.; Toftlund, H.; Wilson, S. R.; Trautwein, A. X.; Winkler, H.; Hendrickson, D. N. *J. Am. Chem. Soc.* **1990**, *112*, 6814. (b) Oshio, H.; Toriumi, K.; Maeda, Y.; Takashima, Y. *Inorg. Chem.* **1991**, *30*, 4252. (c) Conti, J. A.; Chadha, R. K.; Sena, K. M.; Rheingold, A. L.; Hendrickson, D. N. *Inorg. Chem.* **1993**, *32*, 2670. (d) Conti, J. A.; Kaji, K.; Nagano, Y.; Sena, K. M.; Yumoto, Y.; Chadha, R. K.; Rheingold, A. L.; Sorai, M.; Hendrickson, D. N. *Inorg. Chem.* **1993**, *32*, 2681.

(9) Gallois, B.; Real, J. A.; Hauw, C.; Zarembowitch, J. *Inorg. Chem.* **1990**, *20*, 1152.

(10) Real, J. A.; Gallois, B.; Granier, T.; Suez-Panamá, F.; Zarembowitch, J. *Inorg. Chem.* **1992**, *31*, 4972.

(11) Granier, T.; Gallois, B.; Gaultier, J.; Real, J. A.; Zarembowitch, J. *Inorg. Chem.* **1993**, *32*, 5305.

(12) Erickson, N. E.; Sutin, N. *Inorg. Chem.* **1966**, *5*, 1834.

(13) Boudreaux, E. A., Mulay, L. N., Eds. *Theory and Applications of Molecular Paramagnetism*; John Wiley and Sons: New York, 1976.

(14) Sheldrick, G. M. SHELX-86, *Program for Structure Determination*. Univ. of Gottingen, FRG 1986.

(15) Sheldrick, G. M. *System of Computing Programs*. Univ. of Cambridge, Cambridge, England, 1976.

(16) *International Tables for X-ray Crystallography*; Kyoch Press: Birmingham, England, 1974; Vol. 4, p 99.

Table 3. Solvate A Room-Temperature (290 K) and Low-Temperature (135 K) Fractional Atomic Coordinates ($\times 10^4$)[a] and Equivalent Isotropic Thermal Parameters ($Å^2 \times 10^3$) for Non-Hydrogen Atoms

	x/a	y/b	z/c	U_{eq}[b]		x/a	y/b	z/c	U_{eq}[b]
				(a) Room Temperature					
Fe	3133(1)	0912(1)	7656(1)	32(1)	C(103)	−0890(5)	−0206(5)	7477(3)	70(1)
N(1)	3269(4)	3222(4)	8235(2)	33(1)	C(104)	−2502(5)	−0307(5)	7079(3)	49(1)
N(2)	2624(5)	0561(4)	8868(3)	39(1)	N(105)	−2767(5)	0217(5)	6394(5)	49(1)
C(1)	2647(5)	1844(5)	9331(3)	33(1)	C(106)	−1425(5)	0873(5)	6078(3)	39(1)
C(2)	2986(5)	3244(5)	9002(3)	30(1)	C(107)	−1640(6)	1428(5)	5341(3)	51(1)
C(3)	3634(5)	4541(5)	7972(3)	41(1)	C(108)	−0318(6)	2068(5)	4976(3)	54(1)
C(4)	3698(6)	5927(5)	8454(3)	51(1)	C(109)	1278(6)	2136(5)	5360(3)	41(1)
N(5)	3396(5)	5967(5)	9189(3)	48(1)	N(110)	2537(5)	2706(5)	4976(3)	55(1)
C(6)	3018(5)	4604(5)	9470(3)	38(1)	C(111)	3954(6)	2697(6)	5337(3)	55(1)
C(7)	2647(6)	4512(6)	10262(3)	52(1)	C(112)	4249(6)	2196(5)	6105(3)	47(1)
C(8)	2319(6)	3180(6)	10572(3)	58(1)	N(200)	5702(5)	1875(5)	7969(3)	50(1)
C(9)	2347(6)	1822(5)	10118(3)	45(1)	C(200)	7139(6)	2497(5)	8138(3)	45(1)
N(10)	2052(6)	0526(5)	10450(3)	64(1)	S(200)	9130(2)	3384(4)	8413(1)	67(1)
C(11)	2077(6)	−0682(6)	9989(4)	72(1)	N(300)	2838(5)	−1337(5)	7214(3)	51(1)
C(12)	2351(6)	−0691(6)	9199(3)	54(1)	C(300)	2945(5)	−2328(5)	6775(3)	38(1)
N(101)	0435(4)	0459(4)	7175(2)	33(1)	S(300)	3021(2)	−3740(2)	6159(1)	60(1)
N(102)	3012(5)	1664(4)	6474(2)	34(1)	C(400)	1334(7)	4983(7)	3502(4)	93(1)
C(101)	1511(5)	1617(5)	6102(3)	31(1)	C(401)	2175(7)	4318(6)	3028(4)	78(1)
C(102)	0153(5)	0971(5)	6465(3)	32(1)	N(402)	2899(6)	3850(6)	2671(4)	97(1)
				(b) Low Temperature					
Fe	2993(2)	1047(2)	7645(1)	23(1)	C(103)	−0849(10)	−0176(8)	7535(5)	29(3)
N(1)	3232(8)	3169(7)	8164(4)	22(3)	C(104)	−2480(10)	−0290(9)	7127(5)	33(3)
N(2)	2656(8)	0542(7)	8751(4)	26(3)	N(105)	−2785(8)	0195(7)	6431(4)	33(3)
C(1)	2666(9)	1812(9)	9276(5)	26(3)	C(106)	−1425(10)	0897(9)	6102(5)	31(3)
C(2)	2975(9)	3235(8)	8958(5)	24(3)	C(107)	−1592(10)	1431(9)	5344(5)	32(3)
C(3)	3615(9)	4524(8)	7897(5)	26(3)	C(108)	−0268(10)	2065(8)	4986(5)	30(3)
C(4)	3668(10)	5898(9)	8384(5)	33(3)	C(109)	1386(9)	2173(9)	5374(5)	26(3)
N(5)	3390(8)	5970(8)	9143(5)	37(3)	N(110)	2726(8)	2749(7)	5006(4)	31(3)
C(6)	3015(9)	4586(9)	9431(5)	26(3)	C(111)	4142(10)	2696(9)	5397(5)	35(3)
C(7)	2660(9)	4486(9)	10243(5)	27(3)	C(112)	4384(10)	2172(9)	6167(5)	34(3)
C(8)	2338(10)	3142(10)	10557(5)	36(3)	N(200)	5436(9)	1794(7)	7981(4)	33(3)
C(9)	2345(10)	1732(9)	10060(5)	35(3)	C(200)	6924(10)	2410(9)	8159(5)	29(3)
N(10)	2109(9)	0388(8)	10389(4)	39(3)	S(200)	8995(3)	3382(3)	8430(2)	43(2)
C(11)	2116(10)	−0792(10)	9891(5)	40(3)	N(300)	2774(8)	−1056(7)	7167(4)	29(3)
C(12)	2403(10)	−0742(9)	9067(5)	40(3)	C(300)	2910(9)	−2085(9)	6762(5)	32(3)
N(101)	0520(8)	0507(7)	7228(4)	23(3)	S(300)	3041(3)	−3593(3)	6182(1)	36(2)
N(102)	3101(8)	1690(7)	6542(4)	20(3)	C(400)	2143(11)	4339(10)	3019(5)	45(3)
C(101)	1591(10)	1642(8)	6141(5)	27(3)	C(401)	1295(11)	5008(10)	3493(6)	61(3)
C(102)	0167(9)	0991(8)	6492(5)	24(3)	N(402)	2868(10)	3803(9)	2653(5)	56(3)

[a] Numbers in parentheses are estimated standard deviations in the least significant digit. [b] Values for anisotropically refined atoms are given in the form of the equivalent isotropic thermal parameters $U_{eq} = (1/3)(\sum_i \sum_j a_i^* a_j^* \vec{a}_i \vec{a}_j U_{ij})$.

Table 4. Solvate B Room-Temperature (290 K) Fractional Atomic Coordinates ($\times 10^4$)[a] and Equivalent Isotropic Thermal Parameters ($Å^2 \times 10^3$) for Non-Hydrogen Atoms

	x/a	y/b	z/c	U_{eq}[b]		x/a	y/b	z/c	U_{eq}[b]
Fe	6501(1)	2388(1)	1379(1)	68(3)	C(103)	4502(6)	2239(4)	0234(7)	80(9)
N(1)	6122(4)	3322(3)	0234(4)	74(8)	C(104)	3702(6)	1813(5)	−0377(7)	88(9)
N(2)	6320(4)	3495(3)	1843(4)	66(8)	N(105)	3455(4)	1195(4)	−0977(5)	94(9)
C(1)	6233(4)	4264(3)	1373(5)	53(8)	C(106)	4039(6)	0983(4)	−0970(6)	76(9)
C(2)	6134(5)	4072(3)	0508(5)	63(8)	C(107)	3767(6)	0322(4)	−1652(6)	105(9)
C(3)	6050(5)	3260(4)	−0547(6)	86(9)	C(108)	4351(7)	0069(4)	−1648(6)	98(9)
C(4)	5999(5)	3941(4)	−1030(6)	85(9)	C(109)	5202(6)	0426(4)	−0989(6)	74(9)
N(5)	5989(4)	4664(3)	−0793(5)	88(8)	N(110)	5776(5)	0144(3)	−0967(5)	97(9)
C(6)	6069(5)	4744(4)	0024(5)	70(9)	C(111)	6541(6)	0496(4)	−0330(7)	98(9)
C(7)	6060(5)	5516(4)	0312(6)	85(9)	C(112)	6805(5)	1146(4)	0365(6)	83(9)
C(8)	6155(5)	5618(4)	1138(6)	87(9)	N(200)	7776(5)	2524(3)	2134(5)	100(8)
C(9)	6220(5)	4929(4)	1651(6)	66(9)	C(200)	8315(5)	2673(4)	2179(5)	66(8)
N(10)	6266(4)	5031(3)	2434(5)	89(8)	S(200)	9036(2)	2864(2)	2237(2)	132(6)
C(11)	6319(5)	4391(4)	2856(6)	78(9)	N(300)	6858(4)	1785(3)	2618(5)	82(8)
C(12)	6364(5)	3610(4)	2610(5)	65(8)	C(300)	7057(5)	1605(4)	3367(6)	78(9)
N(101)	5095(4)	2011(3)	0281(4)	64(8)	S(300)	7370(2)	1757(2)	4468(2)	128(6)
N(102)	6259(4)	1427(3)	0353(5)	62(8)	C(400)	5000(1)	1502(5)	2500(1)	125(10)
C(101)	5457(6)	1080(4)	−0315(6)	62(9)	C(401)	5000(1)	2368(6)	2500(1)	142(10)
C(102)	4836(5)	1362(4)	−0349(6)	59(9)	N(402)	5000(1)	3057(6)	2500(1)	335(10)

[a] Numbers in parentheses are estimated standard deviations in the least significant digit. [b] Values for anisotropically refined atoms are given in the form of the equivalent isotropic thermal parameters $U_{eq} = (1/3)(\sum_i \sum_j a_i^* a_j^* \vec{a}_i \vec{a}_j U_{ij})$.

Figure 1 shows a perspective drawing of the $[Fe(tap)_2(NCS)_2]$ complex together with the atom-numbering scheme. Each iron atom is surrounded by six nitrogen atoms belonging to two NCS^- groups in the cis position and two tap bidentate ligands. The molecule is chiral, and the unit cell contains one right-handed and one left-handed enantiomer. Interatomic distances and bond angles at room (290 K) and at below (135 K) temperatures are listed in Table 5a.

(i) Ligand Geometries. tap ligands labeled L1 and L2 in Figure 1 are nearly planar, defining their least-squares planes by the

Table 5. Selected Bond Distances (Å) and Angles (deg)[a]

(a) Solvate A

	290 K	135 K
Fe–N(1)	2.225(4)	1.970(7)
Fe–N(2)	2.198(4)	1.982(6)
Fe–N(101)	2.253(4)	1.993(7)
Fe–N(102)	2.180(4)	1.989(6)
Fe–N(200)	2.059(4)	1.927(8)
Fe–N(300)	2.056(4)	1.947(7)
N(300)–C(300)	1.167(7)	1.158(11)
C(300)–S(300)	1.619(5)	1.656(9)
N(200)–C(200)	1.154(7)	1.168(12)
C(200)–S(200)	1.601(6)	1.627(9)
N(1)–Fe–N(2)	76.0(1)	83.3(3)
N(1)–Fe–N(102)	89.0(1)	91.3(3)
N(1)–Fe–N(101)	82.4(1)	87.2(3)
N(101)–Fe–N(102)	74.9(1)	82.4(3)
N(2)–Fe–N(101)	89.3(1)	91.5(3)
N(300)–Fe–N(102)	96.5(2)	90.3(3)
N(300)–Fe–N(101)	95.1(1)	93.4(3)
N(300)–Fe–N(2)	97.7(2)	95.2(3)
N(200)–Fe–N(102)	93.0(2)	91.9(3)
N(200)–Fe–N(1)	87.5(1)	88.7(3)
N(200)–Fe–N(2)	99.9(2)	93.8(3)
N(200)–Fe–N(300)	96.2(2)	90.9(3)
Fe–N(300)–C(300)	156.3(4)	162.4(7)
Fe–N(200)–C(200)	176.1(4)	172.1(7)

(b) Solvate B

Fe–N(1)	2.230(7)	Fe–N(300)	2.046(8)
Fe–N(2)	2.216(6)	N(300)–C(300)	1.132(12)
Fe–N(102)	2.230(7)	C(300)–S(300)	1.635(10)
Fe–N(101)	2.231(8)	N(200)–C(200)	1.184(18)
Fe–N(200)	2.071(10)	C(200)–S(200)	1.586(14)
N(1)–Fe–N(2)	74.3(2)	N(300)–Fe–N(2)	97.7(2)
N(1)–Fe–N(102)	91.5(3)	N(200)–Fe–N(102)	89.0(3)
N(1)–Fe–N(101)	93.6(3)	N(200)–Fe–N(1)	85.1(3)
N(101)–Fe–N(102)	75.1(3)	N(200)–Fe–N(2)	102.6(3)
N(2)–Fe–N(101)	92.4(3)	N(200)–Fe–N(300)	96.8(3)
N(300)–Fe–N(102)	103.5(3)	Fe–N(300)–C(300)	165.4(7)
N(300)–Fe–N(101)	88.6(3)	Fe–N(200)–C(200)	155.6(8)

[a] Numbers in parentheses are estimated standard deviations in the least significant digit.

Table 6. Intermolecular Contacts (Å) Shorter Than van der Waals Distances for Solvate A[a]

	290 K	135 K		290 K	135 K
Intracolumn Contacts					
C(111)···C(107)[1]	3.559	3.543	C(300)···C(108)[1]	3.509	3.374
C(111)···C(106)[1]	3.544	3.588	C(8)···C(4)[2]	3.370	3.342
C(106)···C(110)[1]	3.305	3.313	C(7)···C(6)[2]	3.565	3.467
C(106)···C(109)[1]	3.567	3.544	C(7)···C(2)[2]	3.554	3.493
C(107)···C(109)[1]	3.569	3.495	C(7)···C(200)[2]	3.591	3.538
C(107)···C(100)[1]	3.590	3.541	C(6)···C(6)[2]	3.417	3.393
C(108)···C(100)[1]	3.392	3.369	C(9)···C(4)[2]	3.588	
C(102)···C(108)[1]	3.598	3.561			
Intercolumns Contacts					
C(107)···S(300)[3]	3.568	3.613	S(200)···C(6)[4]	3.290	3.286
C(107)···C(4)[3]	3.504	3.548	C(200)–C(104)[4]	3.162	3.125
C(107)···C(3)[3]		3.555	C(2)···S(200)[4]	3.459	3.453
S(200)···C(103)[4]	3.547	3.434	C(11)···C(8)[5]		3.549
S(200)···C(104)[4]	3.526	3.375			
Solvent–Complex Contacts					
C(112)···C(401)[6]	3.520	3.399	C(104)···N(402)[9]	3.287	3.211
C(3)···N(402)[6]	3.327	3.217	C(300)···C(400)[9]	3.594	3.553
C(400)···C(112)[6]		3.577	C(103)···C(401)[9]		3.535
C(400)···C(107)[7]	3.585	3.517	C(103)···N(402)[9]	3.158	3.090
C(8)···N(402)[8]		3.366			

[a] Key: (1) $-x, -y, -z, 0, 0, 1$; (2) $-x, -y, -z, 1, 1, 2$; (3) $x, y, z, 0, -1, 0$; (4) $x, y, z, -1, 0, 0$; (5) $-x, -y, -z, 0, 0, 2$; (6) $-x, -y, -z, 1, 1, 1$; (7) $-x, -y, -z, 0, 1, 1$; (8) $x, y, z, 0, 0, 1$; (9) $-x, -y, -z, 0, 0, 1$.

positions of the atoms of their central ring C(1), C(2), C(6), C(7), C(8), C(9) (equation of plane $0.8820x + 0.2270y + 0.4130z = 4.9285$) for ligand L1 and C(101), C(102), C(106), C(107), C(108), C(109) (equation of plane $-0.2268x + 0.8238y + 0.5195z = 4.9129$) for ligand L2; the largest deviations observed are 0.064 Å (N(5)) for ligand L1 and 0.122 Å (C(111)) for L2. The NCS$^-$ groups are almost linear (N(200)–C(200)–S(200) = 177.6°, N(300)–C(300)–S(300) = 177.3°) whereas the linkages Fe–NC(S) are bent.

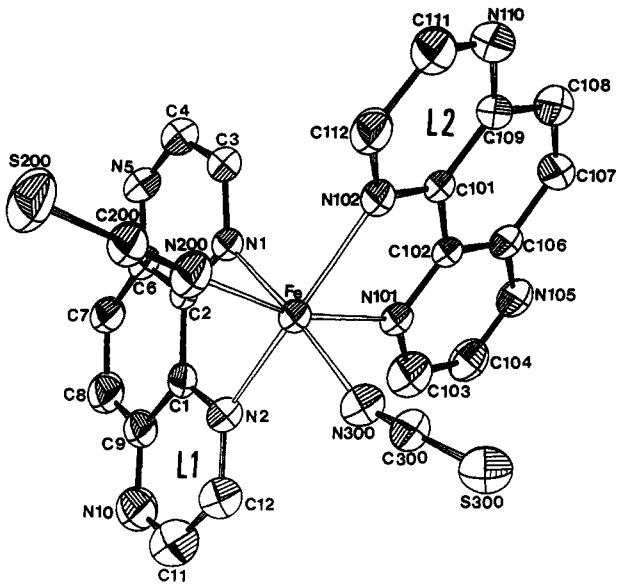

Figure 1. Drawing of the $Fe(tap)_2(NCS)_2$ unit at room temperature. Hydrogen atoms have been omitted for clarity.

(ii) [FeN_6] Octahedron Geometry. The octahedron defined by the six nitrogen atoms around the iron atom has no regular shape with the Fe–N(L) bond lengths being much longer (2.23 Å on average) than that of Fe–N(CS) ones (2.05 Å). Moreover, the geometric constraints of bidentate ligands cause important reduction of the N(tap)–Fe–N(tap) bond angles from the ideal 90° value: N(1)–Fe–N(2) = 76.8°, N(101)–Fe–N(102) = 74.9°. The N(CS)–Fe–N(CS) and N(CS)–Fe–N(tap) angles differ also. This distortion of the [FeN_6] core from O_h symmetry is a common feature of the high-spin-phase structure of $FeL_2(NCS)_2$ compounds, where L is a bidentate ligand (see for example refs 9 and 10), and so is the misorientation of the ligands, relatively to the axes of the octahedron defined by the Fe–N bonds; the N(200)–C(200)–S(200) group is only slightly bent to the Fe–N(200) direction (Fe–N(200)–C(200) = 176.1°), whereas a strong bending is observed in the case of Fe–N(300)–C(300) = 156.3°. Concerning the bidentate ligands, their mean molecular plane, as defined above, makes a slight angle with the Fe–N(tap) bond directions, tap1–Fe–N(1) = 0.8° and tap1–Fe–N(2) = 1.4°, while for the second bidentate ligand tap2–Fe–N(101) = 3.2° and tap2–Fe–N(102) = 3.7°. Finally, the planes defined by tap ligands are 78.4° apart from one another.

(iii) Solvent Inclusion. The acetonitrile molecule is linear (C(400)–C(401)–N(402) = 178.0) and exhibits a slight static disorder; the temperature factors of its atoms are 1.5 times greater than those of the [$Fe(tap)_2(NCS)_2$] unit.

(iv) Crystal Packing. A projection of the crystal structure along the diagonal of the unit cell ($a + b + c$) shows that the crystal packing may be described as a quasi hexagonal arrangement of columns of complex molecules stacking along the ($a + b + c$) direction, with solvent molecules inserted between these columns. A projection perpendicular to the plane defined by the Fe, N(1), and N(2) atoms of a column of complex molecules is shown in Figure 2a, while, in Figure 2b, a projection of such a column is shown projected perpendicularly to the plane defined by the Fe, N(101), and N(102) atoms. Inside a column, a closer packing is achieved by the overlapping of tap ligands of two

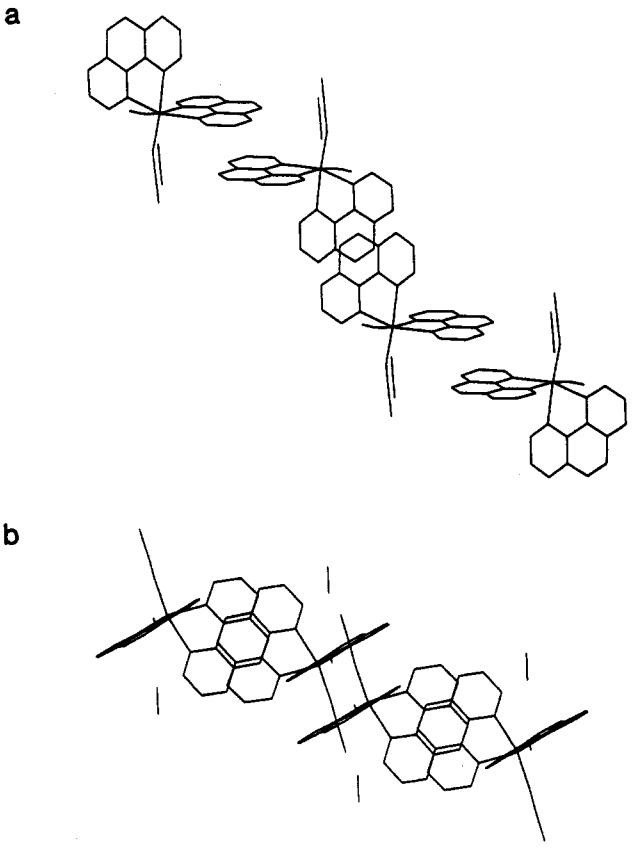

Figure 2. Crystal solvate A: (a) projection of a column of $Fe(tap)_2(NCS)_2$ units perpendicular to the plane defined by the Fe, N(1), and N(2) atoms; (b) projection of the same column perpendicular to the plane defined by the Fe, N(101), and N(102) atoms.

neighboring complex molecules related by an inversion center. The interplanar distances between overlapping tap ligands are short: d(tap1–tap1′) = 3.360 Å and d(tap2–tap2′) = 3.317 Å. The anisotropy of the crystal packing is confirmed by spacial distribution of the intermolecular contacts (interatomic intermolecular distances shorter than the sum of the van der Waals radii are listed in Table 6). They are classified into three kinds: intracolumn contacts, intercolumn contacts, and complex–solvent contacts. It is clear that the greatest amount of intermolecular contacts concerns intracolumn complex molecules: carbon–carbon or carbon–nitrogen contacts.

Structure of A at 130 K. The structure was refined in the $P\bar{1}$ triclinic space group. No drastic change is observed in the molecular configuration of the $[Fe(tap)_2(NCS)_2]$ unit as well as the solvent inclusion. The most important change concerns the $[FeN_6]$ octahedron geometry.

(i) Ligand Geometry. The tap ligands remain planar. The greatest deviations from the least squares plane of the tap1 ligand (equation $0.8852x + 0.2350y + 0.4015z = 4.6966$) are observed for atoms N(10) (0.074 Å), C(11) (0.058 Å), and N(5) (0.060 Å). Concerning tap2 ligand (equation of plane $-0.2323x + 0.8271y + 0.51187z = 4.7486$), the greatest deviations concern atoms C(111) (–0.137 Å), C(112) (–0.127 Å), and C(104) (–0.088 Å). The NCS^- groups remain linear (N(200)–C(200)–S(200) = 178.6°, N(300)–C(300)–S(300) = 178.2°).

(ii) $[FeN_6]$ Octahedron. Fe–N bond lengths are shorter than those observed at room temperature, 1.984 Å on the average for tap ligands (a shortening of 0.230 Å) and 1.937 Å for Fe–N(CS) bonds (a shortening of 0.121 Å). Meanwhile, N–Fe–N bond angles are closer to 90°. As a consequence, the $[FeN_6]$ octahedron is much less distorted than at room temperature (in the high-spin phase). This rearrangement of the octahedron core is accompanied by some change in the bending of the Fe–N(CS) links, Fe–N(200)–(CS) = 172.1° (176.1° at room temperature) and Fe–N(300)–(CS) = 162.4° (156.3° at 290 K). Concerning the tap ligands, the mean molecular planes make a small angle with the Fe–N(tap) directions, (tap1,Fe–N(1)) = 3.1°, (tap1,Fe–N2)) = 3.9°, (tap2,Fe–N(101)) = –5.2°, and (tap2,Fe–N(102)) = –5.6°, and the angle between the two tap ligands (tap1,tap2) = 78.8°, is very close to its room-temperature value.

(iii) Solvent Inclusion. The solvent inclusion remains unchanged at low temperature. The static disorder observed at room temperature is reduced at low temperature, since the equivalent temperature factors of the concerned atoms are, on the average, 30% smaller than at room temperature. Complex–solvent interatomic contacts do not increase noticeably at low temperature.

(iv) Crystal Packing. At low temperature, the number of interatomic intermolecular contacts (Table 6) does not change noticeably. A slight intracolumn shortening and a somewhat reduced interplanar distances between overlapping tap ligands, d(tap1–tap1′) = 3.317 Å and d(tap2–tap2′) = 3.283 Å, are observed. Intercolumn contacts increase very little in number as well (two new contacts out of nine). Let us notice also that these intermolecular contacts do not shorten drastically at low temperature (on average, d(C–C) = 3.53 Å at 290 K, 3.48 Å at 135 K and d(C–S) = 3.48 Å at 290 K, 3.45 Å at 135 K). The contraction of the complex molecule when going from the high-spin to the low-spin state is just compensated by the lattice thermal contraction when going from 290 K to 135 K.

Structure of B at 290 K. Crystal solvate B crystallizes in the $C2/c$ space group. The complex molecule lies on a general position, while the solvent molecule is located on the 2-fold axis. There are eight $[Fe(tap)_2(NCS)_2]$ complex molecules and four CH_3CN units per unit cell. Interatomic distances and bond angles are listed in Table 5b (same atom labeling as for A).

(i) Ligand Geometries. As a general trend, no difference is observed in the bond lengths and bond angles compared with A. The tap ligands are nearly planar: the greatest deviations from the least squares plane of L1 ligand (equation $0.72x + 0.0364y + 0.6843z = 10.2836$) concerns atoms C(11) (0.09 Å) and N(10) (0.062 Å). For L2 ligand (equation of plane $0.2182x + 0.6235y - 0.7507z = 4.228$) greatest deviations are observed for atoms C(112) (–0.11 Å), C(11) (0.07 Å), and N(105) (0.08 Å). As to the NCS^- groups, these are almost linear since the angles N(200)–C(200)–S(200) and N(300)–C(300)–S(300) are 179.3 and 178.5°, respectively, values which are close to those observed in crystal solvate A.

(ii) $[FeN_6]$ Octahedron. The octahedron geometry is not regular, as Fe–N(tap) lengths are longer (2.227 Å on average) than Fe–N(CS) ones (2.059 Å). These distances as well as the bite angles N(1)–Fe–N(2) = 74.3° and N(101)–Fe–N(102) = 75.1° are very close to those of crystal solvate A. One observes that the N(CS)–Fe–N(tap) bond angles are also different from 90° although the values noticeably differ from those observed in crystal solvate A. These angular differences show that at room temperature the distortion of the $[FeN_6]$ octahedron is more pronounced in B than in A. This may be clearly evidenced by considering the trigonal distortion angle Φ as defined previously.[8a] If the two trigonal planes are defined by the groups of atoms N(1), N(102), N(200) and N(2), N(101), N(300), respectively, the following values for Φ are found: 8° and 3.3° for the room- and low-temperature structures, respectively, of A and 15.9° for the room-temperature structure of B. Concerning A, it is clear that the trigonal distortion is reduced at low temperature (0° for a regular octahedron). The value obtained for B, on the other hand, shows that the trigonal distortion is much greater than that of A at room temperature. Another striking difference concerns the ligand orientation relative to the axes of the $[FeN_6]$ octahedron: both NCS^- groups are strongly bent with respect to the corresponding Fe–N links (Fe–N(200)–C(200) = 155.6° and Fe–N(300)–C(300) = 165.4°). Moreover, the mean molecular planes of tap ligands are misoriented relatively to the Fe–N(tap)

Table 7. Intermolecular Contacts (Å) Shorter Than van der Waals Distances for Solvate B[a]

	Intracolumn contacts		
C(107)···C(102)[1]	3.520	C(7)···C(1)[2]	3.565
C(108)···C(101)[1]	3.559	C(7)···C(9)[2]	3.554
C(109)···C(106)[1]	3.521	C(6)···C(9)[2]	3.591
C(8)···C(2)[2]	3.370		
	Intralayer Contacts		
C(112)···N(10)[3]	3.538	C(109)···S(200)[4]	3.608
C(7)···C(300)[3]	3.446	N(105)···C(12)[4]	3.284
S(300)–C(7)[3]	3.557	C(101)···C(200)[4]	3.437
C(102)···S(200)[4]	3.489	C(106)···C(200)[4]	3.336
C(101)···S(200)[4]	3.581	C(104)···C(12)[4]	3.579
C(3)···S(200)[4]	3.626		
	Interlayer Contacts		
C(11)···S(300)[5]	3.586	C(3)···S(200)[5]	3.534
	Solvent–Complex Contacts		
S(300)···N(400)[6]	3.579	C(11)···N(402)[6]	3.375
C(103)···C(401)[6]	3.441	C(400)···N(110)[7]	3.366
C(12)···C(402)[6]	3.080		

[a] Key: (1) $-x, -y, -z$, 1, 0, 0; (2) $-x, -y, -z$, 1, 1, 0; (3) $^1/_2 - x, y - ^1/_2, ^1/_2 - z$, 1, 0, 0; (4) $^1/_2 + x, ^1/_2 - y, z - ^1/_2$; (5) $^1/_2 - x, ^1/_2 - y, -z$, 1, 0, 0; (6) x, y, z; (7) $-x, -y, -z$; 1, 0, 0.

corresponding bond directions ([L1,Fe–N(1)] = –9.54°; [L1,-Fe–N(2)] = –8.07°; [L2,Fe–N(101)] = 3.35°; [L2,Fe–N(102)] = 6.51°). Finally, the planes defined by the L1 and L2 ligands make an angle of 70.6° as compared to 78.4° in the case of A at room temperature.

(iii) Solvent Inclusion. The acetonitrile molecule is found on the 2-fold axis. Carbon–carbon and carbon–nitrogen bond lengths are similar to those observed in A. However, in the present case, the molecule is subject to a strong static disorder which is reflected by the large values of the equivalent temperature factors. In fact, it was not possible, from Fourier map differences, to assign several statistical positions for the concerned atoms, and the refinement of the structure in a lower symmetry group did not improve the final values of the reliability factors.

(iv) Crystal Packing. The crystal packing may be described by columns of complex molecules which stack along the *b* axis and form layers parallel to the (–1,0,1) planes, with solvent molecules inserting between these layers. As for A, the columns are made of complex molecules related by an inversion center. The tap ligands overlap in a different way as compared to A; the interplanar distances, *d*(tap1–tap1′) = 3.444 Å and *d*(tap2–tap2′) = 3.469 Å, are slightly greater than in A. A listing of short contacts is given in Table 7. The number of these contacts relative to atoms belonging to overlapping tap ligands is less important than in A. Short contacts exist also between adjacent columns inside the layers parallel to the (–1,0,1) planes. These are predominantly of the tap–NCS^- type. On the other hand, a few interlayer contacts occur, while solvent–complex contacts are of the same order as in A.

Magnetic Behavior. The temperature dependences of the $\chi_M T$ product obtained in the cooling mode for A and B are shown in Figure 3. The corresponding $\chi_M T$ versus T for $[Fe(phen)_2(NCS)_2]$ is also depicted for comparison. $\chi_M T$ is equal to 3.28 $cm^3\ mol^{-1}\ K$ for A (a value which corresponds to an effective magnetic moment of 5.12 μ_B) at 291 K, and it decreases when cooling down to reach the lower limit of 0.1 $cm^3\ mol^{-1}\ K$ (μ_{eff} = 0.89 μ_B), which is close to the temperature-independent paramagnetism value expected for ls-iron(II) complexes. Consequently, these data clearly indicate that the spin-state transformation is complete both at the highest and lowest temperature. The warming mode gives similar results to the cooling one; in both modes the temperature at which half the transformation is attained corresponds to 168 K. This magnetic behavior indicates a gradual spin-state interconversion for A. Continuous spin-crossovers in solid state involve smaller cooperativity than

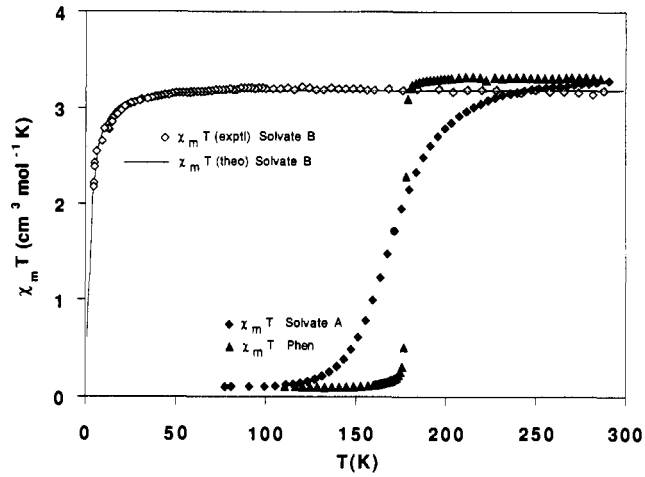

Figure 3. Temperature dependence of $\chi_M T$ for A, B, and $Fe(phen)_2(NCS)_2$ polymorph I. The line was generated using a $S = 2$ axial zero-field-splitting Hamiltonian (D = 7.4 cm^{-1}, g = 2.09, $R = 1.7 \times 10^{-4}$).

discontinuous ones, and a Gibbs–Boltzmann distribution law for molecules in the low-spin state and the thermally accessible high-spin excited state describe in principle the spin conversion; however, reasonably good fits of experimental data have been described only in a few cases.[6b]

The equilibrium between the two electronic states is analyzed with the equilibrium constant determination K_{eq}

$$^1A_1(ls) \overset{K_{eq}}{\leftrightarrow} {}^5T_2(hs)$$

The high-spin to low-spin fraction ratio K_{eq} is determined from $K_{eq} = (\chi_m - \chi_{ls})/(\chi_{hs} - \chi_m)$, where χ_m is the experimental molar magnetic susceptibility at a given temperature, while χ_{hs} and χ_{ls} are the corresponding values of pure high- and low-spin components at the same temperature. K_{eq} is related to the different thermodynamic parameters ΔG, ΔH, and ΔS as follows:

$$\ln K = -\Delta G/RT = -\Delta H/RT + \Delta S/R$$

The spin equilibrium is confirmed when a plot of $\ln K_{eq}$ against $1/T$ is linear to a good approximation in the whole temperature range. In this case, it is possible to get an estimate of ΔH and ΔS (which include electronic and molecular vibrational contributions). The $\ln K_{eq}$ versus $1/T$ plot for A was found to be linear with small deviations in the low-temperature region. The thermodynamic parameters derived from this straight line were ΔH = 15.5 kJ mol^{-1} and ΔS = 92 J $mol^{-1}\ K^{-1}$. Although these values are in agreement with those obtained in the solid state or in solution from systems whose magnetic behavior infer a spin equilibrium,[6b] they are surprisingly greater than the ones obtained from more direct methods, as heat capacity measurements, when the cooperativity is important.[17] These features have been recently pointed out[8c,d] by comparing the results obtained from different methods (magnetic susceptibility and heat capacity measurements) on several $[Fe(3\text{–}OEt\text{–}SalAPA)_2](ClO_4)$ solvates. The authors of this work conclude that it is very difficult to get reliable ΔS and ΔH values by fitting the high-spin molar fraction versus temperature curve. Furthermore, they have doubts about the ability to fit susceptibility data as a criterion to establish whether or not there is any cooperativity in the spin-crossover transformation.

B is high-spin in the whole range of temperature measured. The $\chi_M T$ value is 3.18 $cm^3\ mol^{-1}\ K$ (μ_{eff} = 5.04 μ_B), and it remains practically constant from room temperature to 50 K. This value

(17) (a) Sorai, M.; Seki, S. *J. Phys. Chem. Solids* **1974**, *35*, 555. (b) Claude, R.; Real, J. A.; Zarembowitch, J.; Khan, O.; Ouahab, L.; Grandjean, D.; Boukheddaden, K.; Varret, F.; Dworkin, A. *Inorg. Chem.* **1990**, *29*, 4442.

Table 8. Average Fe–L and Fe–NCS Bond Distances (Å) and Trigonal Distortion Angle Φ (deg) for $Fe(L)_2(NCS)_2$ Compounds

	high-spin form			low-spin form			
	R			*R*			
compd	Fe–L	Fe–NCS	Φ	Fe–L	Fe–NCS	Φ	ref
$Fe(bipy)_2(NCS)_2$[a]	2.173	2.053	14.7	1.966	1.945	7.7	24
$Fe(phen)_2(NCS)_2$[a]	2.206	2.057	13.7	2.009	1.958	8	9
$Fe(btz)_2(NCS)_2$[b]	2.170	2.064	12	1.973	1.948	8.3	10
$Fe(tap)_2(NCS)_2CH_3CN$	2.214	2.057	8	1.983	1.937	3	this work
$Fe(bt)_2(NCS)_2$[c] (form A)	2.202	2.070	15.2				23
$Fe(bt)_2(NCS)_2$[c] (form B)	2.222	2.085	18				23
$Fe(tap)_2(NCS)_2 \cdot {}^1/_2CH_3CN$	2.267	2.058	15.8				this work

[a] These compounds present about a 17% of residual paramagnetism in the low-spin phase. [b] Shows both residual paramagnetism and diamagnetism at low and high temperatures, respectively. [c] Form A has not been characterized at low temperature. Form B does not undergo spin conversion.

is close to that expected for a mononuclear $S = 2$ spin-only iron(II) complex reflecting a more distorted octahedral geometry with respect to A. Below this temperature, the product $\chi_M T$ decreases and attains a value of 2.18 $cm^3\ mol^{-1}\ K$ (μ_{eff} = 4.17 μ_B) at 4.5 K which is smaller than the spin-only value. We have assumed the existence of an axial zero-field-splitting in order to account for the low-temperature region in B. The Hamiltonian used for $S = 2$ is

$$\mathbf{H} = g\beta H\mathbf{S} + D[\mathbf{S}_z^2 - ({}^1/_3)S(S+1)]$$

in which all the variables have their usual meaning. Assuming that $g_\parallel = g_\perp$, we can express the dependence of $\chi_M T$ on T by the relation[18]

$$\chi_\parallel T = \frac{2N\beta^2 g^2}{k}\left[\frac{\exp(x) + 4\exp(-2x)}{\exp(2x) + 2\exp(x) + 2\exp(-2x)}\right]$$

$$\chi_\perp T = \frac{2N\beta^2 g^2}{k}\frac{1}{3x}\left[\frac{9\exp(2x) - 7\exp(x) - 2\exp(-2x)}{\exp(2x) + 2\exp(x) + 2\exp(-2x)}\right]$$

where $\chi_M T = ({}^1/_3)\chi_\parallel T + ({}^2/_3)\chi_\perp T$ and $x = D/kT$. The least-squares fit of experimental data leads to $D = 7.4\ cm^{-1}$, $g = 2.09$, and $R = 1.7 \times 10^{-4}$. R is the agreement factor defined as $\Sigma_i[(\chi_M T)_{obs,i} - (\chi_M T)_{calc,i}]^2/\Sigma_i[(\chi_M T)_{obs,i}]^2$. The value of D is of the order of magnitude of that reported for iron(II) complexes.[19]

Concluding Comments

This work was undertaken to compare the influence that the replacement of two CH groups of 1,10-phenanthroline by two N atoms in $[Fe(phen)_2(NCS)_2]$ complex causes on the spin-state interconversion. The spin conversion in solvate A is continuous and centered around the same temperature as the one of the spin transition in $[Fe(phen)_2(NCS)_2]$, both spin conversions being complete at the highest and lowest temperatures (see Figure 3).

Given that the crystal structure of $[Fe(phen)_2(NCS)_2]$ (polymorph II) was reported,[9] a comparison between this structure and that of solvate A seems appropriate in order to point out the main structural differences which could account for the more or less abrupt character of these spin transformations. At first sight, the molecular geometry in both compounds is very close. No significant differences are observed concerning the tap and phen ligands and the metal surroundings. Although the average value of the Fe–N–C(S) bending angle at room temperature in A is practically identical to that observed in $[Fe(phen)_2(NCS)_2$, the values of the Fe–N–C(S) angles in the former (156.3 and 176.1°) are significantly different compared to those observed in the latter (167°). The most remarkable difference between the two molecular structures deals with the trigonal deformation angle Φ (see Table 8), which is smaller for A in the high- and low-temperature forms according to its less distorted coordination polyhedron (vide infra). The cooperative nature of the spin conversion can be influenced by molecular packing effects which also include the participation of solvent molecules. In this respect, $[Fe(phen)_2(NCS)_2]$ and A exhibit a different packing most likely due to the presence of solvate molecules in A. The former may be described as sheets of complex molecules parallel to *ab* plane; the shortest distances within a sheet are only observed between the carbon atoms of phenanthroline groups. A few significant contacts between consecutive sheets are observed leading to a 2D anisotropic distribution to the intermolecular interactions. As mentioned above, the A packing may be described as a hexagonal arrangement of columns of complex molecules stacked along the $(a + b + c)$ direction. Within a column, interplanar distances between overlapping tap ligands are short and can be considered as π–π interactions. In contrast with the cooperative magnetic behavior differences of both compounds, it is worthwhile noting that for A the intermolecular interactions are greater in number and likely more intense than in $[Fe(phen)_2(NCS)_2]$. In light of these considerations, an unambiguous assignment of the different spin-crossover behaviors to the ligand substitution cannot be done.

Finally, the structural knowledge of the $[Fe(tap)_2(NCS)_2] \cdot nCH_3CN$ (n = 1, $^1/_2$) system allows us to compare the crystal structures of the two forms which exhibit drastic different magnetic properties. This uncommon situation would make possible to estimate, at least in a qualitative fashion, the relevance the different structural factors play on the occurrence of spin-crossover. The values of the average Fe–N bond distances for both $[Fe(tap)_2(NCS)_2]$ solvates are very close, a slight lengthening being observed in B. Owing to how sensitive the spin states of iron(II) complexes are to the electronic and steric effects when Dq is close to the critical values, it is not surprising that spin states can vary with small changes in bond distances and angles. For such small structural modifications and in the context of the ligand field theory, it is assumed that Dq values vary as $1/R^5$, where R is the metal-to-ligand distance. A loss of the ligand field strength in B of about 6% with respect to that of A can be estimated from the $Dq(tap,A)/Dq(tap,B) = (R_B/R_A)^5$ ratio, where R_A and R_B stand for the average Fe–N(tap) bond distance in solvates A and B, respectively. If a resonable value of 1200 cm^{-1} is assumed for Dq(tap,A), a loss in the Dq(tap,B) value of about 70 cm^{-1} results because of bond lengthening.

A similar situation was reported for the spin-crossover compound $[Fe(dppen)_2(Cl)_2] \cdot 2(CH_3)_2CO$ (where dppen = 1,2-bis(diphenylphosphino)ethylene).[20] It remains high-spin after the loss of solvent. Both forms (solvated and unsolvated) crystallize in different space groups, but in spite of the similar molecular organization that they exhibit, a significant change in the molecule orientation most likely due to the solvent inclusion was observed. This fact should be the cause of the small changes observed in the Fe–P and Fe–Cl bond distances. Furthermore, an order–disorder phase transition involving the solvent molecules simultaneously accompanies the spin-conversion and, as has been suggested, probably triggers the spin-crossover behavior.[21] A

(18) O'Connor, C. J. *Prog. Inorg. Chem.* **1982**, *29*, 203.
(19) Carlin, R. L. *Magnetochemistry*; Springer Verlag: Berlin, 1986.
(20) Cecconi, M.; Di Vaira, M.; Midollini, S; Orlandini, A.; Saccconi, L. *Inorg. Chem.* **1981** *20*, 3423.

more surprising situation was found in the $[Fe(bt)_2(NCS)_2]$ compound[22] (bt = 2,2′-bi-2-thiazoline) which crystallizes as two different polymorphs depending on the temperature of the solvent evaporation. Both forms, named I (spin-crossover) and II (paramagnetic), crystallize in the same space group with small differences in the cell parameters. The molecular structures are rather similar (see Table 8) exhibiting only slight differences in bond distances and angles. In order to understand the cooperative mechanism of the first-order spin transition in I and the paramagnetic behavior in II, the authors based their discussion mainly on the differences in the molecular packing. Intermolecular interactions have been invoked only as the cause of the different magnetic properties between both forms in the later examples. However, as for the $[Fe(tap)_2(NCS)_2]$ system the differences in metal-to-ligand bond distances would justify a loss of Dq at least of the same order or magnitude and could account for the different magnetic behaviors of both forms in each system.

Another factor to be taken into account is the relative magnitude of the trigonal deformation angle Φ. Relevant structural parameters involved in the spin conversion for a series of $[Fe(L)_2(NCS)_2$ complexes are gathered in Table 8. A careful examination of these data shows that, for the complexes which undergo spin conversion, the Φ values depend on the amount of hs form attaining the smallest value in the pure ls phase which suggests this type of distortion may be coupled to spin interconversion. This fact was recently noted in the complex $[Fe(tpen)](ClO_4)_2 \cdot {}^2/_3H_2O$ (tpen = *N,N,N′,N′*-tetrakis(2-pyrydyl)-1,2-ethylenediamine).[8a] Besides, the Φ value is greater for the forms which do not undergo spin conversion. All these facts fit well with the analysis of the distortion effect along a trigonal twisting coordinate on the energies of the ^1A, ^3T, and ^5T states for $Fe(phen)_3^{2+}$ which was carried out a long time ago.[23] It foresees a crossing of $S = 0$ and $S = 2$ states about midway along the pseudorotational coordinate although, to reach the crossover point, only a fraction of the full rotation would be required. Then, it can be concluded that differences in the trigonal distortion and bond distances may be the main cause of the different magnetic behaviors between the two forms of the $[Fe(tap)_2(NCS)_2]$ and $[Fe(bt)_2(NCS)_2]$ compounds.

Acknowledgment. This work was supported by the Comision Interministerial de Ciencia y Tecnología (Project PB91-0807-C02-01). We are very grateful to Dr. J. Zarembowitch for her help with magnetic measurements. One of us (M.C.M.) is indebted to the Consellería de Cultura, Educació i Ciencia de la Generalitat Valenciana, for a grant.

Supplementary Material Available: Tables of X-ray data collection characteristics, complete bond distances, bond angles anisotropic thermal parameters for non-hydrogen atoms, and calculated fractional positions and isotropic thermal parameters for hydrogen atoms are listed in Tables SI–SIX (9 pages). Ordering information is given on any current masthead page.

(21) König, E.; Ritter, G.; Kulshreshtha, S. K.; Waigel, J.; Sacconi, L. *Inorg. Chem.* **1984**, *23*, 1241.
(22) Ozarowski, A.; McGarvey, B. R.; Sarkar, A. B.; Drake, J. E. *Inorg. Chem.* **1988**, *27*, 628.
(23) Purcell, K. F. *J. Am. Chem. Soc.* **1979**, *101*, 5147.
(24) Konno, M.; Mikami-Kido, M. *Bull. Chem. Soc. Jpn.* **1991**, *64*, 339.